

RAPIDLY RISING OPTICAL TRANSIENTS FROM THE BIRTH OF BINARY NEUTRON STARS

KENTA HOTOKEZAKA¹, KAZUMI KASHIYAMA^{2,3}, AND KOHTA MURASE^{4,5,6,7}¹Center for Computational Astrophysics, Flatiron Institute, 162 5th Ave, New York, NY 10010, USA²Department of Physics, the University of Tokyo, Bunkyo, Tokyo 113-0033, Japan³Research Center for the Early Universe, the University of Tokyo, Tokyo 113-0033, Japan⁴Department of Physics, The Pennsylvania State University, University Park, PA 16802, USA⁵Department of Astronomy & Astrophysics, The Pennsylvania State University, University Park, PA 16802, USA⁶Center for Particle and Gravitational Astrophysics, The Pennsylvania State University, University Park, PA 16802, USA⁷Yukawa Institute for Theoretical Physics, Kyoto University, Kyoto 606-8502, Japan

ABSTRACT

We study optical counterparts of a new-born pulsar in a double neutron star system like PSR J0737-3039A/B. This system is believed to eject a small amount of mass of $\mathcal{O}(0.1M_{\odot})$ at the second core-collapse supernova. We argue that the initial spin of the new-born pulsar can be determined by the orbital period at the time when the second supernova occurs. The spin angular momentum of the progenitor is expected to be similar to that of the He-burning core, which is tidally synchronized with the orbital motion, and then the second remnant may be born as a millisecond pulsar. If the dipole magnetic field strength of the nascent pulsar is comparable to that inferred from the current spin-down rate of PSR J0737-3039B, the initial spin-down luminosity is comparable to the luminosity of super-luminous supernovae. We consider thermal emission arising from the supernova ejecta driven by the relativistic wind from such a new-born pulsar. The resulting optical light curves have a rising time ~ 10 days and peak luminosity $\sim 10^{44}$ erg/s. The optical emission may last for a month to several months, due to the reprocessing of X-rays and UV photons via photoelectric absorption. These features are broadly consistent with those of the rapidly-rising optical transients. The high spin-down luminosity and small ejecta mass are favorable for the progenitor of the repeating fast radio burst, FRB 121102. We discuss a possible connection between newborn double pulsars and fast radio bursts.

Keywords: supernovae: general — pulsars: general — binaries : close —

1. INTRODUCTION

The double pulsar, PSR J0737-3039A/B, is one of the most important stellar objects for studying compact stars and gravity (Lyne et al. 2004; Kramer et al. 2006). Such a double pulsar system eventually merges due to gravitational-wave emission, which is one of the main targets of ground-based gravitational-wave detectors, Advanced LIGO/Virgo and KAGRA. Binary neutron stars are also considered to produce a short gamma-ray burst (GRB) at the merger (Eichler et al. 1989). While the orbital parameters of this system and the pulsar characteristics have been well-studied, the formation path is still a mystery (e.g., Postnov & Yungelson 2014 for a recent review). The current orbital and proper motion imply that the second core-collapse supernova, which formed the younger pulsar PSR J0737-3039B, was an ultra-stripped supernova associated with a very small amount of mass ejection of $\mathcal{O}(0.1M_{\odot})$ (Piran & Shaviv 2005;

Dall’Osso et al. 2014). Furthermore, van den Heuvel (2007); Beniamini & Piran (2016) pointed out that a majority of the observed double neutron star systems in the Galactic plane originate from ultra-stripped supernovae.

A small amount of ejecta suggests that supernovae associated with double pulsar formation are fainter than normal core-collapse supernovae if the emission powered only by the radioactivity of ^{56}Ni and ^{56}Co (Tauris et al. 2013; Suwa et al. 2015; Moriya et al. 2017). However, the spin-down power of new-born pulsars may be much higher than the radioactive power. With the observed magnetic field strength of PSR J0737-3039B and its initial spin estimated via the assumption of the tidal synchronization, the second supernova may leave a fast-rotating pulsar as a compact remnant. Then, the emission of supernovae associated with the double pulsar formation like PSR J0737-3039A/B is likely powered by the pulsar wind, as considered in the pulsar-driven model

for super-luminous supernovae (Kasen & Bildsten 2010; Woosley 2010).

Recent high-cadence optical transient surveys have discovered rapidly evolving transients (e.g., Drout et al. 2014; Arcavi et al. 2016; Tanaka et al. 2016). Some of these transients may arise from the core collapse of an ultra-stripped star. For instance, Arcavi et al. (2016) find rapidly rising optical transients, which have a rise time scale of 10 days or even shorter and peak luminosities between 10^{43} – 10^{44} erg/s. These luminosities are in between those of typical type II and super-luminous supernovae. The nickel mass required to explain their peak luminosity exceeds the total ejecta mass inferred from the rise time, suggesting that there is an extra energy source in addition to the radioactivity.

Such pulsar-driven supernovae become of interest in view of possible connections with fast radio bursts (FRBs). It has been predicted that a bright long-term radio emission may naturally arise from synchrotron emission of non-thermal electrons and positrons in a pulsar wind nebula (Murase et al. 2016). The repeating FRB 121102 discovered by the Arecibo telescope (Spitler et al. 2016), whose host galaxy was recently identified following the FRB detection of *Very Large Array* (VLA), is accompanied by a persistent radio counterpart that is possibly associated with the FRB source (Chatterjee et al. 2017; Tendulkar et al. 2017). A young pulsar with a high spin-down luminosity surrounded by a small amount of supernova ejecta has been argued as one of the plausible candidates of the radio source (Kashiyama & Murase 2017).

In this work, we explore optical counterparts of the formation of double pulsar systems such as PSR J0737-3039A/B. We estimate the ejecta mass of the second supernovae and an initial spin period and magnetic field strength of the associated remnant in §2. Then we study the optical emission leaking from the supernova ejecta powered by the pulsar wind in §3. In §4, we discuss the possible connection of the young binary neutron stars with repeating FRBs. In §5, we conclude our results and discuss the observational implications.

2. MILLISECOND PULSARS ARISING FROM ULTRA-STRIPPED PROGENITORS IN CLOSE BINARIES

2.1. Observational characteristics of the known double pulsar system PSR J0737-3039A/B

The radio observations of PSR J0737-3039A/B provide us implications for their progenitors and the second core-collapse supernova, where the younger pulsar of the system was formed. Here we summarize some relevant parameters inferred from the observations.

PSR J0737-3039A/B is a double pulsar system of

which the neutron star masses are $1.338^{+0.0007}_{-0.0007}M_{\odot}$ and $1.249^{+0.0007}_{-0.0007}M_{\odot}$ and the current orbital period is 0.102 day with an orbital eccentricity of 0.088 (Lyne et al. 2004; Kramer et al. 2006). The current spin periods of PSR J0737-3039A and B are 23 ms and 2.8 s, respectively¹. The proper motion of the system is also measured as ~ 9 km/s (Kramer et al. 2006; Deller et al. 2009). These orbital parameters and proper motion suggest that the mass ejection at the second core collapse M_{ej} is only 0.1 – $0.2M_{\odot}$ (e.g., Piran & Shaviv 2005; Dall’Osso et al. 2014). This very small amount of the ejecta requires that the progenitor was an ultra-stripped star. Beniamini & Piran (2016) showed that a majority of the observed double neutron star systems in the Galactic disk originate from ultra-stripped progenitors (see also van den Heuvel 2007).

The spin-down rate of the pulsars indicates that the current magnetic field strengths are $10^{9.8}\text{G}$ and $10^{12.2}\text{G}$ for PSR J0737-3039A and B, respectively (Lyne et al. 2004). The fast spin and weak magnetic field of PSR J0737-3039A suggest that this pulsar was formed first and experienced mass accretion from the companion. Therefore, PSR J0737-3039B is considered to be formed at the second core collapse. Note that the current magnetic field strengths may be weaker than their initial strengths because the magnetic fields might have decayed. We focus on such the second core-collapse event associated with the formation of PSR J0737-3039B-like objects throughout the paper.

In addition to the double pulsar system PSR J0737-3039A/B, PSR J1906+0746 is likely to be the younger pulsar in a close neutron star binary with an orbital period of 0.17 day (Lorimer et al. 2006; van Leeuwen et al. 2015). The magnetic field strength and the ejecta mass at the second core collapse are estimated as $10^{12.2}\text{G}$ and $\sim 0.8M_{\odot}$, respectively (Lorimer et al. 2006; Beniamini & Piran 2016). Note, however, that this ejecta mass is estimated based on the upper limit on the proper motion $\lesssim 400$ km/s of this system, so that it could be smaller (van Leeuwen et al. 2015).

2.2. A progenitor scenario

We consider the following scenario of the double neutron star formation (see Tauris et al. 2013, 2015; Suwa et al. 2015 for the evolution of ultra-stripped progenitors):

1. A He star with a mass $\sim 3M_{\odot}$ orbits with an orbital period of ~ 0.1 day around a neutron star that is formed at the first supernova. In such a system, the He star is quickly tidally synchronized

¹ PSR J0730-3039B has not been seen from the Earth since 2008.

with the orbital motion, as will be discussed later.

2. After the core He-burning finishes, the tidal torque on the star is significantly reduced since the convective core contracts. While the angular momentum of the envelope is lost due to the wind mass loss during this stage, the angular momentum of the core may not be significantly transferred to the envelope (Hirschi et al. 2005; Yoon & Langer 2005; Meynet & Maeder 2007).
3. At the end of the stellar evolution, the second supernova occurs, where a small amount of mass $\mathcal{O}(0.1M_\odot)$ is ejected. The newly formed pulsar rotates with the angular momentum of the core prior to the collapse. This rotational energy is the source of a supernova powered by a pulsar wind discussed in the following sections.

Here we make two simple but reasonable assumptions. First, the spin angular momentum and mass of the core just prior to the core collapse is assumed to be equal to those of the He-burning core. Second, we assume a circular orbit until the core collapse. Then, the initial spin period of PSR J0737-3039B, $P_{s,ns}$, can be estimated through the angular momentum conservation:

$$\begin{aligned}
 P_{s,ns} &= \left(\frac{r_{g,c} R_c}{r_{g,ns} R_{ns}} \right)^2 P_{orb}, \\
 &\approx 0.8 \text{ ms} \left(\frac{r_{g,c}^2}{0.075} \right)^{-1} \left(\frac{r_{g,ns}^2}{0.4} \right) \left(\frac{R_c}{0.13R_\odot} \right)^{-2} \\
 &\quad \times \left(\frac{R_{ns}}{11\text{km}} \right)^2 \left(\frac{P_{orb}}{0.12 \text{ day}} \right), \quad (1)
 \end{aligned}$$

where R_c and R_{ns} are the radius of the core of the He star and of the new-born pulsar, $r_{g,c}$ and $r_{g,ns}$ are their non-dimensional gyroradii (Kushnir et al. 2016; Lattimer & Prakash 2001), P_{orb} is the orbital period at the second core collapse. Here we have used the semi-major axis at the second collapse of $\sim 10^{11}$ cm (Beniamini et al. 2016), inferred from that the second core-collapse supernova occurred at ~ 50 Myr ago, corresponding to the spin-down age of PSR J0737-3039B. Note that the above estimate of the pulsar's spin frequency is the maximal one since we have assumed that the core does not lose its angular momentum in the post He-burning phase. For instance, the initial spin period of the pulsar becomes ~ 8 ms if 90% of the core's spin angular momentum is lost. The initial spin energy

of the new-born pulsar is

$$\begin{aligned}
 E_s &= \frac{1}{2} r_{g,ns}^2 R_{ns}^2 M_{ns} \left(\frac{2\pi}{P_{s,ns}} \right)^2, \\
 &\approx 2.5 \cdot 10^{52} \text{ erg} \left(\frac{r_{g,c}^2}{0.075} \right)^2 \left(\frac{r_{g,ns}^2}{0.4} \right)^{-1} \left(\frac{M_{ns}}{1.3M_\odot} \right) \\
 &\quad \times \left(\frac{R_{ns}}{11 \text{ km}} \right)^{-2} \left(\frac{R_c}{0.13R_\odot} \right)^4 \left(\frac{P_{orb}}{0.12 \text{ day}} \right)^{-2}, \quad (2)
 \end{aligned}$$

where M_{ns} is the mass of the new-born pulsar. Note that this energy is much larger than the explosion energy of a typical supernova of $\sim 10^{51}$ erg.

The assumption of the synchronization during the core He-burning phase is justified as follows. The tidal synchronization of the progenitor star occurs on the synchronization time (Zahn 1975, 1977; Kushnir et al. 2017):

$$\begin{aligned}
 t_{sync} &\approx 300 \text{ yr } q^{-5/6} \left(\frac{1+q}{2} \right)^2 \left(\frac{r_g^2}{0.075} \right) \left(\frac{P_{orb}}{0.12 \text{ day}} \right)^{17/3} \\
 &\quad \times \left(\frac{R_*}{0.43R_\odot} \right)^2 \left(\frac{R_c}{0.13R_\odot} \right)^{-9} \left(\frac{M_*}{3M_\odot} \right) \left(\frac{M_c}{1.4M_\odot} \right)^{4/3} \quad (3)
 \end{aligned}$$

where q is the mass ratio of the progenitor star to the companion neutron star, R_* and M_* are the radius and mass of the He star, and M_c is the core mass. This time scale is much shorter than the time scale of the life time and of the wind angular-momentum loss of a He star. Thus, the progenitor star is tidally synchronized during the He-star phase. It can be also shown that the circularization of the orbit occurs during the He-burning phase due to the tidal torque (Zahn 1977). In the post He-burning phase, the core radius shrinks, and hence the tidal synchronization is much less efficient so that the progenitor star likely leaves the synchronization state (see Eq. 3 for the strong dependence of the synchronization time on the convective core radius). The situation is somewhat complicated for binaries with longer orbital periods. For instance, double neutron star progenitors with a gravitational-merger time of $t_{GW} = 10$ Gyr, corresponding to $P_{orb} = 0.65$ day, have $t_{sync} \approx 3$ Myr, which is of order of the time scale of the stellar evolution.

Note that the synchronization time scale is quite sensitive to the structure of the progenitors so that the stellar evolution calculation is needed for detailed studies (see, e.g., Tauris et al. 2015 for a stellar evolution study of double neutron stars). Furthermore, the spin angular momentum of the core may be lost during the late stage of the stellar evolution. The final spin angular momentum of the core depends on the efficiency of angular momentum losses from the star due to the wind and that from the stellar core to the envelope. The former depends on the

anisotropy and the magnetization of the wind (see, e.g., [Meynet & Maeder 2007](#); [Ud-Doula et al. 2009](#)). The latter occurs through the angular momentum transport due to the magnetic field and meridional circulation. Note that [Hirschi et al. \(2005\)](#); [Yoon & Langer \(2005\)](#); [Meynet & Maeder \(2007\)](#) showed that the angular momentum exchange between the core and envelope may not be efficient in the post core He-burning phase. We do not go into these issues in this work and will address them in a future work.

3. OPTICAL EMISSION FROM PULSAR-DRIVEN ULTRA-STRIPPED SUPERNOVAE

A new-born pulsar of a binary neutron star system launches a relativistic wind, which interacts with the supernova ejecta surrounding the wind. The forward shock in the supernova ejecta and the reverse shock in the wind (the wind termination shock) are formed. The internal energy of the supernova ejecta is increased via the shock dissipation and the reprocess of non-thermal radiation from the pulsar wind. Here we consider an optical transient arising from such a system (see, e.g., [Kotera et al. 2013](#); [Kasen et al. 2016](#); [Kashiyama et al. 2016](#)).

3.1. Dynamical and thermal evolution of the system

Pulsar winds are powered by the pulsar's spin-down energy with a luminosity ([Spitkovsky 2006](#)):

$$L_{\text{sd}} \approx \frac{\mu^2}{c^3} \left(\frac{2\pi}{P_{\text{s,ns}}} \right)^4, \\ \approx 2.2 \cdot 10^{44} \text{ erg/s} \left(\frac{B}{10^{12.5} \text{ G}} \right)^2 \left(\frac{P_{\text{s,ns}}}{1 \text{ ms}} \right)^{-4}, \quad (4)$$

where $\mu = BR_{\text{ns}}^3/2$, B is the dipole magnetic field strength at the neutron star surface at the dipole pole, and we have assumed that the dipole axis is aligned to the rotational axis of the star. Here we have also assumed that the current strength of the magnetic field of PSR J0737-3039B is a typical value of new-born pulsars in close double neutron star systems. The spin-down luminosity is constant until the spin-down time:

$$t_{\text{sd}} = \frac{E_s}{L_{\text{sd}}}, \\ \approx 2.3 \text{ yr} \left(\frac{B}{10^{12.5} \text{ G}} \right)^{-2} \left(\frac{P_{\text{s,ns}}}{1 \text{ ms}} \right)^2, \quad (5)$$

After t_{sd} , the spin-down luminosity declines as $\propto t^{-2}$. Note that we focus on the evolution of the system and its optical emission up to 100 days after the explosion, and hence, the spin-down luminosity is constant for our fiducial parameters.

The energy flux of the pulsar wind is carried by relativistic particles and magnetic fields:

$$L_{\text{sd}} = L_{e^+e^-} + L_B, \\ \equiv (1 + \sigma)L_{e^+e^-}, \quad (6)$$

where $L_{e^+e^-}$ and L_B are the luminosities of electrons/positrons and magnetic fields, respectively. The ratio of the luminosities between these two components are traditionally denoted by a parameter σ . The out-going energy flux near the pulsar is dominated by the magnetic field, i.e., $\sigma \gg 1$. Then the magnetic energy is assumed to be converted to the particles' energy due to either magnetic reconnection or plasma/magnetohydrodynamical instabilities around the wind termination shock. As in the previous works for pulsar-driven supernovae (e.g., [Murase et al. 2015](#); [Kashiyama et al. 2016](#)) we consider the limit $\sigma \ll 1$, i.e., $L_B \ll L_{e^+e^-}$, in the nebula just outside the wind termination shock. This is motivated by the one-zone modeling of the Crab pulsar wind nebula (see, e.g., [Rees & Gunn 1974](#); [Kennel & Coroniti 1984](#)).

Thermal emission emerging from the supernova ejecta powered by a pulsar wind is described by the first law of thermodynamics of the ejecta ([Arnett 1979](#); [Kasen & Bildsten 2010](#)):

$$\frac{dE_{\text{int}}}{dt} = -\frac{E_{\text{int}}}{t} - L_{\text{rad}} + \dot{Q}, \quad (7)$$

where E_{int} is the internal energy, L_{rad} is the thermal radiation cooling rate, and \dot{Q} is the heating rate of the ejecta. Here we describe the thermal radiation cooling as $L_{\text{rad}} \approx E_{\text{int}}/t_{\text{rad}}$, where $t_{\text{rad}} = 3\xi\kappa M_{\text{ej}}/4\pi v_{\text{ej}}ct$ is the photon diffusion time scale at a given time, κ is the opacity of the ejecta to the thermal photons, v_{ej} is the typical ejecta velocity, ξ is a geometrical factor depending on the ejecta profile.

We turn now to discuss the heating rate \dot{Q} and the dynamics of the ejecta. As long as the supernova ejecta is sufficiently optically thick, the spin-down power injected to the ejecta forms a forward shock in the ejecta irrespective of the value of σ . During this phase, roughly a half of the spin-down energy is converted to the internal energy and another half is converted to the kinetic energy. The energy dissipation at the forward shock is efficient until the time when the thermal radiation efficiently escapes from the system² or the total injected energy becomes comparable to the ejecta's initial kinetic energy. The former occurs when the diffusion time of

² The synchrotron cooling time of relativistic electrons and positrons injected in the wind nebula is faster than the dynamical time (see, e.g., [Metzger et al. 2014](#); [Murase et al. 2015](#)). Therefore the pressure in the wind nebula is dominated by radiation. Once the radiation starts to diffuse out from the system, the pulsar wind may not push the supernova ejecta efficiently.

thermal photons in the ejecta is comparable to the expansion time:

$$t_{\text{diff}} = \left(\frac{3\xi\kappa M_{\text{ej}}}{4\pi c v_{\text{ej}}} \right)^{1/2},$$

$$\approx 5 \text{ day } \xi^{1/2} \left(\frac{\kappa}{0.1 \text{ cm}^2/\text{g}} \right)^{1/2}$$

$$\times \left(\frac{M_{\text{ej}}}{0.1 M_{\odot}} \right)^{3/4} \left(\frac{E_{\text{sn}}}{10^{50} \text{ erg}} \right)^{-1/4}, \quad (8)$$

where we use the opacity as the sum of the electron scattering of partially ionized plasma and the bound-bound absorption, and ξ is chosen to be unity. Here the supernova kinetic energy $E_{\text{sn}} = 10^{50}$ erg corresponds to the initial ejecta velocity of $v_{\text{ej},0} \approx 0.03c$ and the ejecta mass of $M_{\text{ej}} \approx 0.1 M_{\odot}$. The latter occurs at the sweep-up time t_{sw} , which is estimated by

$$\eta M_{\text{ej}} v_{\text{ej}}^2 \approx \int_0^{t_{\text{sw}}} L_{\text{sd}} dt \approx t_{\text{sw}} L_{\text{sd}}, \quad (9)$$

where η is an order-of-unity parameter that depends on the ejecta's structure (Suzuki & Maeda 2017). The sweep-up time is thus

$$t_{\text{sw}} \approx 10 \text{ day } \eta \left(\frac{B}{10^{12.5} \text{ G}} \right)^{-2}$$

$$\times \left(\frac{P_{\text{s,ns}}}{1 \text{ ms}} \right)^4 \left(\frac{E_{\text{sn}}}{10^{50} \text{ erg}} \right). \quad (10)$$

The supernova ejecta expands with a constant velocity until $t \sim t_{\text{sw}}$. After t_{sw} , the injected energy from the pulsar wind exceeds E_{sn} and the ejecta velocity increases with time if $t_{\text{diff}} > t_{\text{sw}}$. We describe the shock heating rate as

$$\dot{Q}_{\text{sh}}(t) \approx \frac{1}{2} L_{\text{sd}} \quad (\text{for } t \leq t_{\text{sw}}, t_{\text{diff}}). \quad (11)$$

For $t > t_{\text{sw}}$, the shock proceeds in the outer part of the ejecta, where the density gradient is rather steep (Chevalier & Soker 1989). In such a region, the shock heating is less efficient compared to those due to the irradiation by non-thermal photons produced in the pulsar wind nebula as discussed later. Here we neglect the shock heating for $t > t_{\text{sw}}$ (see Kasen et al. 2016 for the shock heating rate in the ejecta). Furthermore, t_{sw} is longer than t_{diff} for the parameters considered in this paper (see Table 1). In such cases, the forward shock breaks out by t_{sw} . After the shock breaks out, the energy injection into the ejecta due to the shock is weakened and radiative cooling becomes quite efficient. As a result, the ejecta is slowly accelerated due to the adiabatic expansion and the momentum injection. These may result in the increase of the ejecta velocity by $\lesssim 50\%$ at 100 days. However, we simply assume that the ejecta velocity is constant with time in this work because we

do not solve the X-ray and UV absorptions of the ejecta at late times properly (see the following discussion).

The heating due to the reprocessing of non-thermal photons produced in the nebula can be efficient even at late times. Here we treat these processes in a simple way as follows. At early times, electromagnetic cascades proceed in the saturation regime, leading to a flat energy spectrum up to ~ 1 MeV (Metzger et al. 2014). At later times, the spectrum depends on the seed photon spectra, but it can roughly be estimated to be a flat spectrum from ~ 1 eV to ~ 0.1 TeV while the supernova emission continues (e.g., Murase et al. 2015). High-energy γ rays ($\gtrsim 1$ MeV) heat up the ejecta through the Compton scattering and the pair production process. X-ray and UV photons are absorbed and heat up the ejecta through the photoelectric (bound-free) absorption unless the ejecta are fully ionized. Here we describe the heating rate as

$$\dot{Q}_{\text{rad}}(t) \approx (f_{\gamma} + f_{\text{x-uv,bf}}) L_{\text{sd}}, \quad (12)$$

where f_{γ} and $f_{\text{x-uv,bf}}$ are the thermalization efficiencies of γ rays and X-ray and UV photons to the spin-down luminosity, respectively. We calculate the frequency dependent thermalization efficiency of γ rays at each time:

$$f_{\gamma}(t) = \frac{\int_{\nu_{\text{min}}}^{\nu_{\text{max}}} \frac{d\nu}{\nu} \min(K_{\gamma,\nu} \tau_{\gamma,\nu}, 1)}{\int_{1 \text{ eV}}^{1 \text{ TeV}} \frac{d\nu}{\nu}}, \quad (13)$$

where the frequency range of γ rays is $(h\nu_{\text{min}}, h\nu_{\text{max}}) = (10 \text{ keV}, 1 \text{ TeV})$, and h is the Planck constant. Here, $\tau_{\gamma,\nu}$ is the optical depth of the ejecta to γ rays and $K_{\gamma,\nu}$ is the photon inelasticity at a given frequency, where the Klein-Nishina cross section and the cross section for the Bethe-Heitler pair production in the electric field of a carbon nucleus are taken into account (Murase et al. 2015; Chodorowski et al. 1992). Note that the coefficient of the γ -ray optical depth depends on the density profile of the ejecta. Here we simply assume a density profile to be constant with the radius. Adopting a realistic density profile may result in different ejecta mass and velocity estimates by a factor of a few.

The thermalization efficiency of X-ray and UV photons ($\sim 10 \text{ eV}$ to $\sim 10 \text{ keV}$) is somewhat more difficult to estimate because it depends on the ionization state of the ejecta. The value of $f_{\text{x-uv,bf}}$ is limited by the energy fraction of photons with energies from $\sim 10 \text{ eV}$ to $\sim 10 \text{ keV}$, and hence, $f_{\text{x-uv,bf}} \lesssim 1/4$. In this work, we assume $f_{\text{x-uv,bf}}$ to be constant with time and we determine $f_{\text{x-uv,bf}}$ such that the late-time tail of the theoretical light curve reproduces the observed light curves (see Table 1). Note that the photoelectric absorption is efficient until the supernova ejecta are fully ionized. The ionization break occurs at different times for different frequencies. For instance, the ionization break-out

Table 1. Parameters of theoretical light curves

Event	redshift	κ [cm ² /g]	M_{ej} [M_{\odot}]	v_{ej} [c]	E_{sn} [erg]	L_{sd} [erg/s]	$f_{\text{X-UV,bf}}$
PTF10iam	0.109	0.1	0.1	0.07	$4.4 \cdot 10^{50}$	$2.4 \cdot 10^{44}$	0.9
SNLS04D4ec	0.593	0.1	0.1	0.09	$7.3 \cdot 10^{50}$	$2.9 \cdot 10^{44}$	0.05
SNLS05D2hk	0.699	0.1	0.1	0.06	$3.2 \cdot 10^{50}$	$3.2 \cdot 10^{44}$	0.1
SNLS06D1hc	0.555	0.1	0.1	0.07	$4.4 \cdot 10^{50}$	$2.6 \cdot 10^{44}$	0.1

The redshifts are taken from [Arcavi et al. \(2016\)](#).

time for iron can be estimated as ([Metzger et al. 2014](#)):

$$t_{\text{bo}} \approx 100 \text{ day} \left(\frac{M_{\text{ej}}}{0.1 M_{\odot}} \right) \left(\frac{v_{\text{ej}}}{10^9 \text{ cm/s}} \right)^{-3/2} \left(\frac{T}{10^5 \text{ K}} \right)^{-0.4} \\ \times \left(\frac{X_{\text{Fe}}}{0.35} \right)^{1/2} \left(\frac{L_{\text{sd}} t}{1.7 \cdot 10^{51} \text{ erg/s}} \right)^{-1/2} \left(\frac{Z}{26} \right)^{3/2}, \quad (14)$$

where X_{Fe} is the mass fraction of iron of the ejecta ([Suwa et al. 2015](#)). The ionization break time of the lighter elements is shorter, thereby $f_{\text{X-UV,bf}}$ may decrease with time on a timescale of ~ 100 days in a realistic situation.

In summary, a supernova ejecta powered by a pulsar wind is heated by (i) the forward shock in the ejecta until $t \approx \min(t_{\text{diff}}, t_{\text{sw}})$, (ii) the Compton scattering and pair production process to γ rays emitted by non-thermal electrons and positrons in the pulsar wind nebula, which last until the ejecta becomes optically thin to γ rays, and (iii) the photoelectric absorption of X-ray and UV photons, which likely lasts until 100 days. This injected energy into the ejecta is cooled by the adiabatic expansion and radiative losses. Note that we neglect the radioactive heating as it is expected to be much smaller than the spin-down luminosities for our fiducial parameters. The resulting bolometric light curve of the thermal radiation is obtained as

$$L_{\text{rad}}(t) \approx \frac{\exp\left(-\frac{t^2}{2t_{\text{diff}}^2}\right)}{t_{\text{diff}}^2} \int^t dt \dot{Q}(t) \exp\left(\frac{t^2}{2t_{\text{diff}}^2}\right), \quad (15)$$

where we have assumed that the ejecta are not accelerated significantly, and the initial internal energy of the supernova ejecta does not contribute to the radiation. The latter is justified because the adiabatic cooling is efficient for compact progenitors.

Figure 1 shows the bolometric light curve of the thermal emission L_{rad} and the total heating rate. The heating rate of each process is also depicted. Here we use the parameters of PTF10iam shown in Table 1. The bolometric light curve arises on the diffusion time scale and has a peak luminosity of $\approx L_{\text{sd}}/2$. It declines fast from t_{diff} to 20 days, where the Compton scattering and pair production dominate the heating rate and γ rays start to leak from the ejecta on this time scale. After 20 days, the bound-free absorption to X-ray and UV

photons dominates the heating rate, which contributes to the long-lasting tail of the bolometric light curve.

3.2. Optical light curves

We calculate bolometric light curves of the supernova thermal radiation using Eq. (7). In order to obtain the light curve at a given frequency, we assume the black-body spectrum with a temperature given by $T_{\text{eff}} = (L_{\text{rad}}/4\pi\sigma_{\text{SB}}r^2)^{1/4}$, where σ_{SB} is the Stefan-Boltzmann constant ([Arnett 1979](#)). For instance, the effective temperature at the peak time $\approx t_{\text{diff}}$ with the peak luminosity $\approx L_{\text{sd}}/2$ is

$$T_{\text{eff}} \approx 4 \cdot 10^4 \text{ K} \left(\frac{B}{10^{12.5} \text{ G}} \right)^{0.5} \left(\frac{P_{\text{s,ns}}}{1 \text{ ms}} \right)^{-1} \\ \times \left(\frac{v_{\text{ej}}}{0.03 \text{ c}} \right)^{-1/2} \left(\frac{t_{\text{diff}}}{5 \text{ day}} \right)^{-1/2}. \quad (16)$$

We expect bright thermal radiation in the UV to optical bands after the peak time. The black-body assumption cannot be justified once the photosphere shrinks significantly. This occurs shortly after the peak of the bolometric light curve. Then the emission is dominated by the nebular emission rather than the photospheric emission. However, the calculation of the nebular emission requires detailed treatments on the radiative transfer, which are beyond the scope of this paper.

Figure 2 shows the light curves of the thermal emission arising from the pulsar-driven supernova with small ejecta mass. And also shown are the observed light curves of rapidly rising optical transients ([Arcavi et al. 2016](#)). The peak luminosity and rise time scale are basically determined by L_{sd} and $\kappa M_{\text{ej}}/v_{\text{ej}}$, respectively. The slope of the tail depends on $f_{\text{X-UV,bf}}$ and v_{ej} . The parameters used for each event are listed in Table 1. These parameter ranges are inferred from the formation scenario of double pulsar systems like PSR J0737-3039A/B, as described in the previous section. Note that we have four independent parameters, κM_{ej} , v_{ej} , L_{sd} , and $f_{\text{X-UV,bf}}$, to generate the theoretical light curves. It is worthy to note that the observed data are reproduced with the ejecta's kinetic energies of $3\text{--}8 \cdot 10^{50}$ erg, which are consistent with the results of a hydrodynamical simulation of ultra-stripped supernovae ([Suwa et al.](#)

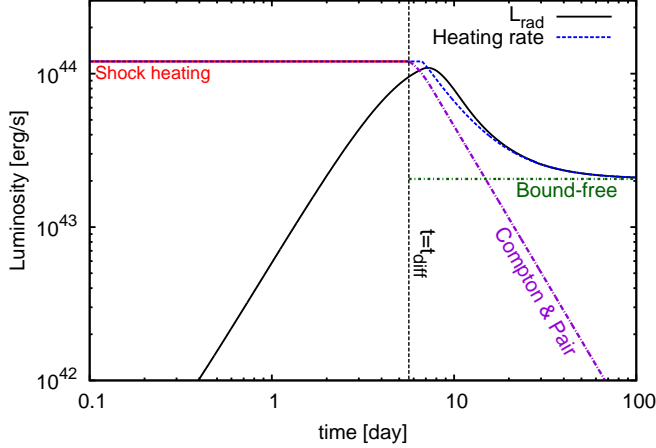


Figure 1. The bolometric light curve (black solid curve) and heating rates. The ejecta mass, initial kinetic energy of the ejecta, and the spin-down luminosity of the newborn pulsar are chosen to be $0.1M_{\odot}$, $4.4 \cdot 10^{50}$ erg, and $2.4 \cdot 10^{44}$ erg/s, respectively. The heating rates due to the shock, γ rays through the Compton scattering and pair production, and bound-free absorption are shown as a red solid, purple short dot-dashed, and green long dot-dashed curve, respectively. Also shown as a vertical line is the diffusion time of thermal photons.

2015). Around 100 days, the ejecta temperature becomes somewhat low ~ 3000 K, where atoms with low ionization energies, e.g. iron, are not fully recombined (Kleiser & Kasen 2014). The thermalization efficiency of the photoelectric absorption $f_{X-UV,bf}$ is 0.05 to 0.1, corresponding to that roughly less than a half of the energy in X-ray and UV photons is thermalized. Note that, however, the back-body assumption may not be a good approximation at late times, so that the values of $f_{X-UV,bf}$ derived via the light curve fitting are physically less meaningful.

In summary, an optical counterpart of the double pulsar formation like PSR J0737-3039A/B, i.e., an ejecta mass of $\sim 0.1M_{\odot}$ and a pulsar’s initial spin-down luminosity of $\sim 2 \cdot 10^{44}$ erg/s, has a fast rise time, bright peak luminosity, and long-lasting tail, which broadly agree with the observed light curves of the rapidly rising optical transients (Arcavi et al. 2016). The late-time energy injection to the ejecta due to the photoelectric absorption plays a crucial role to produce the long-lasting tail of the light curves. In order to reproduce the observed light curves, one needs a spin-down luminosity of $\gtrsim 2 \cdot 10^{44}$ erg/s and a spin down time of $\gtrsim 0.3$ yr, respectively. These conditions give upper limits on the initial spin period and magnetic field strength as ~ 3 ms and $10^{13.5}$ G, respectively.

3.3. Rates and diversity

The rate of ultra-stripped supernovae powered by a new-born pulsar in a double pulsar system is expected

to be $\sim 0.1\%$ of that of normal core-collapse supernovae. This number is estimated from the population of double neutron stars in the Galaxy (Kalogera et al. 2004; Kim et al. 2015), as well as the rate of short GRBs (with a correction of the beaming factor; Wanderman & Piran 2015). While the rate of rapidly rising optical transients is still unknown, the inferred rate of $\sim 10^2 \text{ Gpc}^{-3} \text{ yr}^{-1}$ looks consistent with this rate.

The formation of double pulsars likely has variations in the orbital period at the second core collapse and the strength of the magnetic field. Note also that, as we mentioned earlier, the initial spin period of pulsars depends on the mass loss history of the post He-burning phase. Therefore we expect there to be a broad range of the peak luminosities and rise times (see Kashiyama et al. 2016 for a study with a wide range of parameters of new-born pulsars). For instance, the spin-down luminosity of a pulsar in a binary with an orbital period of 0.65 days, corresponding to a merger time of 10 Gyr, is $\sim 3 \cdot 10^{41}$ erg/s, if the progenitor star is tidally synchronized during the core He-burning phase. In such a case, the radioactivity of ^{56}Ni may provide more energy than the pulsar wind at the peak time of the light curve, and hence, the peak luminosity is much fainter. Such population may explain some of the observed faint ultra-stripped supernovae and calcium-enriched gap transients (Moriya et al. 2017).

4. CONNECTION BETWEEN FAST RADIO BURSTS AND DOUBLE PULSAR SYSTEMS?

We now turn to discuss a scenario that the new-born pulsars in close double neutron stars are the progenitors of FRBs. Young neutron star systems have been intensively investigated as the FRB sources (e.g., Popov & Postnov 2010; Cordes & Wasserman 2016; Connor et al. 2016; Murase et al. 2016), and even more so for the repeating FRB 121102 after the discovery of its host galaxy and persistent radio counterpart. Several authors claim that a high spin-down luminosity and/or small ejecta mass are favored to explain the observed characteristics of FRB 121102 (Kashiyama & Murase 2017; Metzger et al. 2017; Kisaka et al. 2017; Katz 2017; Dai et al. 2017; Piro & Burke-Spolaor 2017; Waxman 2017). In particular, Kashiyama & Murase (2017) showed that the persistent radio counterpart is consistent with the radio emission arising from a pulsar wind nebula in an ultra-stripped supernova remnant with $M_{ej} \sim 0.1 M_{\odot}$, powered by a new-born pulsar with $B \sim 10^{12}\text{--}10^{13}$ G, $P_{s,ns} \lesssim$ a few ms, and an age of ~ 10 yr. The above parameters are in accord with those of new-born pulsars in close double neutron stars.

The population of repeating FRB sources can be estimated as follows. The rate of repeating FRBs inferred from the survey is $5.1_{-4.8}^{+17.8}$.

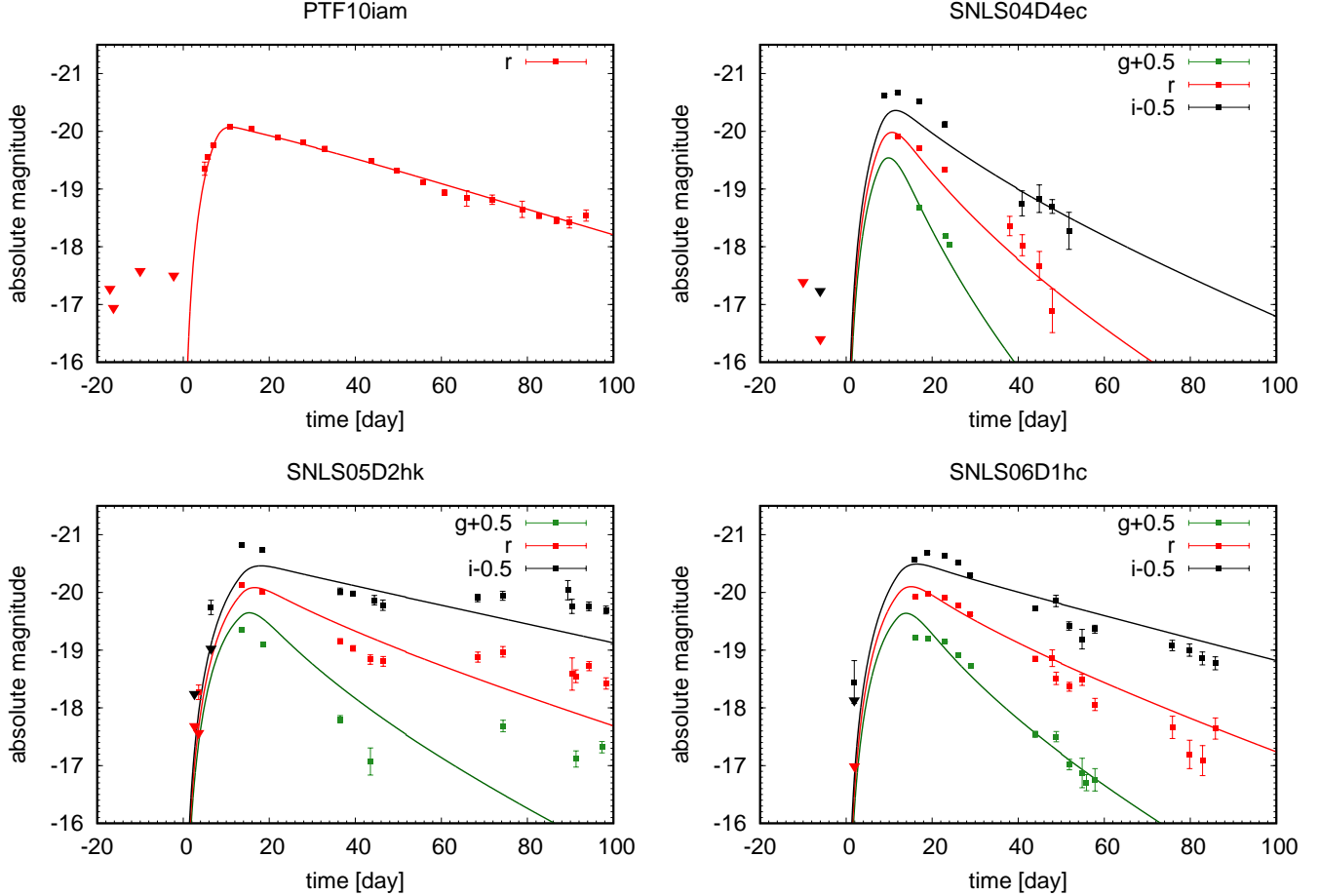


Figure 2. Absolute magnitude of the optical emission from a supernova ejecta powered by a new-born pulsar wind and the observed data of the rapidly-rising optical transients taken from [Arcavi et al. \(2016\)](#). The detections and the 3-sigma upper limits are depicted as squares and triangles, respectively. Here we take the effect of the cosmological redshift on the observed time and observed flux into account for the theoretical curves. The parameters of the theoretical curves used for each event are listed in Table 1.

$10^4 \text{ sky}^{-1} \text{ day}^{-1}$ ([Scholz et al. 2016](#)). Given the fact that 11 bursts are detected in 0.6 day and repeating FRBs are detectable by the Arecibo telescope at distances out to $\sim 1 \text{ Gpc}$, the formation rate of repeating FRB sources is roughly estimated to be $\sim 60 f_b^{-1} \text{ Gpc}^{-1} \text{ yr}^{-1} (\mathcal{T}_{\text{FRB}}/10 \text{ yr})^{-1}$. Here \mathcal{T}_{FRB} is a typical lifetime of repeating FRB objects and $f_b \leq 1$ is a beaming factor of them. If $\mathcal{T}_{\text{FRB}} \sim 10 \text{ yr}$, the rate is compatible with the formation rate of binary neutron stars (see, e.g., [Kalogera et al. 2004](#); [Kim et al. 2015](#) for the Galactic double neutron star systems and [Wanderman & Piran 2015](#) for short GRBs).

While the rate of rapidly rising optical transients is currently unknown, more systematic observational studies will allow us to reveal the event rate. This will enable us to test our scenario. Furthermore, if millisecond pulsars formed in neutron star binaries are the progenitor of the rapidly rising optical transients, bright radio pulses and persistent emission are expected to be associated with these events. Therefore the radio follow-up

observations of these transients can confirm or rule out this scenario. Also, successful detections will allow us to discover extragalactic pulsars with millisecond periods.

While the scenario has some testable predictions, we should note that the host property of FRB 121102 is so far against the possible connection between rapidly rising transients and repeating FRBs; the host galaxy of FRB 121101 is a dwarf-star-forming galaxy ([Tendulkar et al. 2017](#)) while those of the rapidly rising transients are massive galaxies ([Arcavi et al. 2016](#)). We definitely need more samples for this discussion too.

5. SUMMARY AND DISCUSSION

We studied optical counterparts of a new-born pulsar in double neutron star systems like PSR J0737-3039A/B. We considered the thermal emission arising from a pulsar wind embedded in the supernova ejecta. Given the ejecta mass, magnetic field's strength of the pulsar inferred from the PSR J0737-3039A/B, and its initial spin, which is inferred from the tidal synchroniza-

tion of the progenitor star during the core He-burning phase, this emission is expected to have a peak bolometric luminosity of $\sim 10^{44}$ erg/s and a rise time of ~ 10 days. In addition, the optical light curves have a long-lasting tail due to the photoelectric absorption of the ejecta to X-ray and UV photons emitted by the pulsar wind nebula. These features are broadly consistent with those of the observed rapidly rising optical transients (Arcavi et al. 2016).

There are several issues in our model. Regarding the pulsar model of ultra-stripped supernovae, one of the concerns is that the broad emission and absorption lines of $H\alpha$ are seen in the spectrum of PTF10iam, which are not expected for the explosion of ultra-stripped progenitors. However, it might be possible to be explained by Si II so that more detailed studies of the spectra are needed (Arcavi et al. 2016). While we argued that tidal synchronization may lead to a fast-rotating pulsar as a remnant of the second supernova, initial magnetic fields are highly uncertain and stronger magnetic fields are possible. One should also note that the initial spin frequency, i.e., the initial spin down luminosity, of PSR J0737-3039B may be much lower than our estimate, depending on the mass loss history of the progenitor. In order to address this issue, detailed studies based on the stellar evolution are needed.

We also discussed the possible connection between young binary neutron stars and FRBs. A small amount of the ejecta and high pulsar spin-down luminosity at the birth of the younger pulsars of binary neutron stars are in accord with the parameters for the repeating FRB 121102 (Kashiyama & Murase 2017). Furthermore, the formation rate of repeating FRBs seems consistent with that of binary neutron stars. These suggest that young pulsars of binary neutron stars may produce FRBs.

While this work focused on electromagnetic counterparts of new-born neutron star binaries, analogous ar-

guments can be made for other nascent systems such as black hole-neutron star binaries and black hole binaries. In particular, a massive progenitor star that is tidally synchronized by the companion may lead to outflow-driven transients via the long-lasting accretion onto a new-born black hole at the second collapse (Kimura et al. 2017). The spin evolution of compact binary progenitors is imprinted in the spin parameters of merging binary black holes, which can also be measured through gravitational-wave detections (Abbott et al. 2016). Such measurements will shed lights on various questions on the formation scenario of compact binary objects that have been golden candidate sources of gravitational waves (Kushnir et al. 2016; Rodriguez et al. 2016; Zaldarriaga et al. 2017; Hotokezaka & Piran 2017).

Apart from the emission of the ejecta powered by the pulsar wind, we expect there to be significant non-thermal radiation from the pulsar wind nebula. This non-thermal radiation has a broad spectrum from the radio to X and γ rays. These are also bright counterparts of a new-born pulsar in close double neutron star systems. We will discuss this nebular emission and its detectability in a separate paper. It is also worthy to note that extragalactic binary pulsars can be a standard cosmological siren, which may allow us to measure the expansion rate of the Universe (Seto et al. 2001).

We thank Jason Hessels, Brian Metzger, Masaru Shibata, Anatoly Spitkovsky, and Ko Takahashi for useful discussion. We are grateful to Iair Arcavi for providing us the observational data of rapidly-rising transients. K. H. is supported by Flatiron Fellowship at the Simons Foundation. K. K. acknowledges financial support from JST CREST. The work of K. M. is supported by NSF grant No. PHY-1620777.

REFERENCES

- Abbott, B. P., Abbott, R., Abbott, T. D., et al. 2016, *Physical Review X*, 6, 041015
- Arcavi, I., Wolf, W. M., Howell, D. A., et al. 2016, *ApJ*, 819, 35
- Arnett, W. D. 1979, *ApJL*, 230, L37
- Beniamini, P., Hotokezaka, K., & Piran, T. 2016, *ApJL*, 829, L13
- Beniamini, P., & Piran, T. 2016, *MNRAS*, 456, 4089
- Chatterjee, S., Law, C. J., Wharton, R. S., et al. 2017, *Nature*, 541, 58
- Chevalier, R. A., & Soker, N. 1989, *ApJ*, 341, 867
- Chodorowski, M. J., Zdziarski, A. A., & Sikora, M. 1992, *ApJ*, 400, 181
- Connor, L., Sievers, J., & Pen, U.-L. 2016, *MNRAS*, 458, L19
- Cordes, J. M., & Wasserman, I. 2016, *MNRAS*, 457, 232
- Dai, Z. G., Wang, J. S., & Yu, Y. W. 2017, *ApJL*, 838, L7
- Dall’Osso, S., Piran, T., & Shaviv, N. 2014, *MNRAS*, 438, 1005
- Deller, A. T., Bailes, M., & Tingay, S. J. 2009, *Science*, 323, 1327
- Drout, M. R., Chornock, R., Soderberg, A. M., et al. 2014, *ApJ*, 794, 23
- Eichler, D., Livio, M., Piran, T., & Schramm, D. N. 1989, *Nature*, 340, 126
- Hirschi, R., Meynet, G., & Maeder, A. 2005, *A&A*, 443, 581
- Hotokezaka, K., & Piran, T. 2017, *ArXiv e-prints*:1702.03952
- Kalogera, V., Kim, C., Lorimer, D. R., et al. 2004, *ApJL*, 601, L179
- Kasen, D., & Bildsten, L. 2010, *ApJ*, 717, 245
- Kasen, D., Metzger, B. D., & Bildsten, L. 2016, *ApJ*, 821, 36
- Kashiyama, K., & Murase, K. 2017, *ApJL*, 839, L3
- Kashiyama, K., Murase, K., Bartos, I., Kiuchi, K., & Margutti, R. 2016, *ApJ*, 818, 94
- Katz, J. I. 2017, *ArXiv e-prints*:1703.04226
- Kennel, C. F., & Coroniti, F. V. 1984, *ApJ*, 283, 694
- Kim, C., Perera, B. B. P., & McLaughlin, M. A. 2015, *MNRAS*, 448, 928

- Kimura, S. S., Murase, K., & Mészáros, P. 2017, ArXiv e-prints:1702.07337
- Kisaka, S., Enoto, T., & Shibata, S. 2017, ArXiv e-prints:1702.02922
- Kleiser, I. K. W., & Kasen, D. 2014, MNRAS, 438, 318
- Kotera, K., Phinney, E. S., & Olinto, A. V. 2013, MNRAS, 432, 3228
- Kramer, M., Stairs, I. H., Manchester, R. N., et al. 2006, Science, 314, 97
- Kushnir, D., Zaldarriaga, M., Kollmeier, J. A., & Waldman, R. 2016, MNRAS, 462, 844
- . 2017, MNRAS, 467, 2146
- Lattimer, J. M., & Prakash, M. 2001, ApJ, 550, 426
- Lorimer, D. R., Stairs, I. H., Freire, P. C., et al. 2006, ApJ, 640, 428
- Lyne, A. G., Burgay, M., Kramer, M., et al. 2004, Science, 303, 1153
- Metzger, B. D., Berger, E., & Margalit, B. 2017, ArXiv e-prints:1701.02370
- Metzger, B. D., Vurm, I., Hascoët, R., & Beloborodov, A. M. 2014, MNRAS, 437, 703
- Meynet, G., & Maeder, A. 2007, A&A, 464, L11
- Moriya, T. J., Mazzali, P. A., Tominaga, N., et al. 2017, MNRAS, 466, 2085
- Murase, K., Kashiyama, K., Kiuchi, K., & Bartos, I. 2015, ApJ, 805, 82
- Murase, K., Kashiyama, K., & Mészáros, P. 2016, MNRAS, 461, 1498
- Piran, T., & Shaviv, N. J. 2005, Physical Review Letters, 94, 051102
- Piro, A. L., & Burke-Spolaor, S. 2017, ArXiv e-prints:1703.03013
- Popov, S. B., & Postnov, K. A. 2010, in Evolution of Cosmic Objects through their Physical Activity, ed. H. A. Harutyunian, A. M. Mickaelian, & Y. Terzian, 129–132
- Postnov, K. A., & Yungelson, L. R. 2014, Living Reviews in Relativity, 17, 3
- Rees, M. J., & Gunn, J. E. 1974, MNRAS, 167, 1
- Rodriguez, C. L., Zevin, M., Pankow, C., Kalogera, V., & Rasio, F. A. 2016, ApJL, 832, L2
- Scholz, P., Spitler, L. G., Hessels, J. W. T., et al. 2016, ApJ, 833, 177
- Seto, N., Kawamura, S., & Nakamura, T. 2001, Physical Review Letters, 87, 221103
- Spitkovsky, A. 2006, ApJL, 648, L51
- Spitler, L. G., Scholz, P., Hessels, J. W. T., et al. 2016, Nature, 531, 202
- Suwa, Y., Yoshida, T., Shibata, M., Umeda, H., & Takahashi, K. 2015, MNRAS, 454, 3073
- Suzuki, A., & Maeda, K. 2017, MNRAS, 466, 2633
- Tanaka, M., Tominaga, N., Morokuma, T., et al. 2016, ApJ, 819, 5
- Tauris, T. M., Langer, N., Moriya, T. J., et al. 2013, ApJL, 778, L23
- Tauris, T. M., Langer, N., & Podsiadlowski, P. 2015, MNRAS, 451, 2123
- Tendulkar, S. P., Bassa, C. G., Cordes, J. M., et al. 2017, ApJL, 834, L7
- Ud-Doula, A., Owocki, S. P., & Townsend, R. H. D. 2009, MNRAS, 392, 1022
- van den Heuvel, E. P. J. 2007, in American Institute of Physics Conference Series, Vol. 924, The Multicolored Landscape of Compact Objects and Their Explosive Origins, ed. T. di Salvo, G. L. Israel, L. Piersant, L. Burderi, G. Matt, A. Tornambe, & M. T. Menna, 598–606
- van Leeuwen, J., Kasian, L., Stairs, I. H., et al. 2015, ApJ, 798, 118
- Wanderman, D., & Piran, T. 2015, MNRAS, 448, 3026
- Waxman, E. 2017, ArXiv e-prints:1703.06723
- Woosley, S. E. 2010, ApJL, 719, L204
- Yoon, S.-C., & Langer, N. 2005, A&A, 443, 643
- Zahn, J.-P. 1975, A&A, 41, 329
- . 1977, A&A, 57, 383
- Zaldarriaga, M., Kushnir, D., & Kollmeier, J. A. 2017, ArXiv e-prints:1702.00885